Journal of Colloid and Interface Science 685 (2025) 555–564

Contents lists available at ScienceDirect

Journal of Colloid And Interface Science

journal homepage: www.elsevier.com/locate/jcis

Regular Article

Upcycling of photovoltaic waste graphite into high performance graphite anode

Jianjiao Xiong [a,1], Yanfeng Wang [a,1], Jijun Lu [a,*], Fengshuo Xi [a], Zhongqiu Tong [a], Wenhui Ma [b], Shaoyuan Li [a,*]

[a] Faculty of Metallurgical and Energy Engineering, Key Laboratory of Complex Nonferrous Metal Resources Clean Utilization, Kunming University of Science and Technology, Kunming 650093 China
[b] School of Engineering, Yunnan University, Kunming 650500 China

HIGHLIGHTS

- Proposed flash joule heating method that directly converts PV WG to FWG in milliseconds.
- Ultra-high temperature removes the impurities and increases the graphitization degree.
- Ordering structure and increasing layer spacing are favorable for Li^+ transport.
- The FWG anode exhibited superior reversible capacity (413 mAh g^{-1}) and long-cycle stability.

GRAPHICAL ABSTRACT

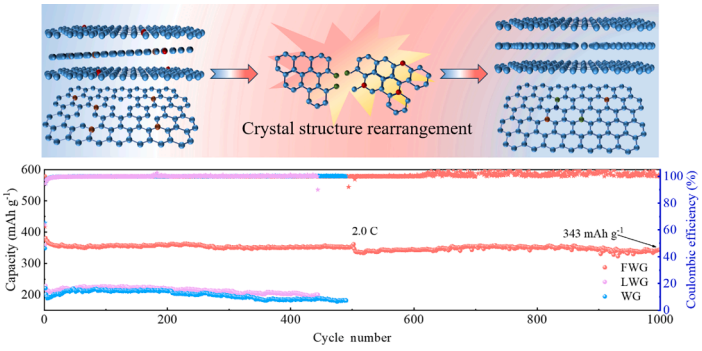

ARTICLE INFO

Keywords:
Photovoltaic waste graphite
Flash joule heating
Upcycling graphite anodes
High-rate performance
Targeted regeneration

ABSTRACT

High-value recycling of photovoltaic waste graphite (WG) is an effective path to achieve “carbon neutrality”. However, the current most adopted methods are landfilling, incineration and leaching, which can lead to undesirable environmental contamination and waste of resources. Here, an energy-efficient and high-value flash recycling strategy is developed in which photovoltaic WG is converted to high-capacity and high-rate graphite anode for lithium-ion batteries (LIBs) in milliseconds. Ultra-high temperatures (>3000 K) were provided by flash joule heat to remove harmful impurities in the PV waste graphite, while improving the graphitization degree of WG and the (002) layer spacing of WG, making the upcycled graphite more suitable for lithium-ion (Li^+) intercalation and deintercalation. The upcycled graphite as a lithium-ion battery anode exhibits high reversible capacity (~413 mAh g^{-1}) and robust cycling stability (>90.1 % retention at 2.0C rate for 1000cycles), which is superior to the current state-of-the-art commercial graphite anode. Overall, this work provides a feasible approach for the sustainable management of photovoltaic waste graphite, contributing to cleaner production and circular economy in the photovoltaic industry.

* Corresponding authors.
E-mail addresses: jjlu@kust.edu.cn (J. Lu), lsy415808550@163.com (S. Li).
[1] Equal contribution to this work.

https://doi.org/10.1016/j.jcis.2025.01.175
Received 29 September 2024; Received in revised form 3 January 2025; Accepted 19 January 2025
Available online 21 January 2025

1. Introduction

Recently, led by the global "carbon peaking and carbon neutrality" policy, the Photovoltaic (PV) industry has become one of the important areas of global energy transition [1]. According to the International Energy Agency analysis, the global total installed capacity of PV reached 1552.3 GW in 2023, and is forecasted to reach 1954.6 GW in 2024 [2]. By 2025, the global annual power generation of renewable energy will exceed that of coal, becoming the largest source of electricity in the world [3]. The speedy development of the PV industry has driven the continuous growth of the demand for raw materials [4]. Graphite is an important consumable in the hot field system of monocrystalline silicon growth and polysilicon ingot casting furnace, that relate to its good conductivity, thermal conductivity, corrosion resistance [5]. In 2023, the output of China's PV monocrystalline silicon reached 478.6 GW, and the demand for PV graphite reached about 175,000 tons (at 0.36 t/MW). However, PV graphite is prone to cracking under the effect of alternating thermal stresses and electromagnetic forces in the hot field system, which need to be replaced periodically. That result in large amounts of graphite being retired every year [6]. Currently, less attention has been paid to those waste graphite, and most of that is directly disposed of in landfills or simple leaching treatment, which inevitably causes problems such as environmental and resource waste [7]. How to realize the green and efficient recycling of PV waste graphite (WG) is a key step for the green development of PV industry.

With the deepening of the concept of green and sustainable development, lithium-ion batteries (LIBs) are rapidly becoming the mainstream energy storage devices in the consumer electronics industry and new energy vehicle market out of the high energy density and long cycle life [8]. Graphite has been become the mainstream product of anode materials for LIBs owing to its advantages of low voltage platforms of indeintercalation lithium, excellent conductivity and low price [9]. It is estimated that 285 million tons of the battery-grade graphite will be required by 2035 [10]. Knowing that untreated graphite-based materials cannot be directly used as anode, and impurity removal and high-temperature graphitization are required [11,12]. Considering the non-renewable characteristics and the current situation of high-cost graphitization process of graphite material, there is an urgent need for alternative graphite-based materials to alleviate the pressure on the supply chain of battery-grade graphite [13]. With the isotropic and crystallinity adjustable, the PV WG is expected to be used as graphite anode to alleviate energy shortage [14]. However, there are still some impurities and structural defects that hinder the intercalation and deintercalation of lithium-ion (Li^+) when applied to the LIBs, which needs to be upgraded and reconstructed.

Ultra-high temperature can effectively evaporate to remove volatile impurities, and enlarged the (002)-layer spacing, which made the regenerated graphite more suitable for de-embedded lithium [15,16]. Meanwhile, the ultra-high temperature (>3000 K) realizes high graphitization conversion of carbon-based materials. As a highly efficient heating method, flash joule heating (FJH) technology can realize milliseconds of rapid heating and cooling without the need for additional solvents and catalysts, which has become an important means for the preparation of energy materials, high entropy alloys, recycling solid waste recently [17–19]. Herein, the upcycling of WG using flash joule heating is expected to realize its value-added recycling for the preparation of high-performance graphite anodes.

Here, we propose a FJH method that directly converts cheap photovoltaic WG to high-performance FWG anode. This method provide a ultra-high temperature (~ 3500 K) less than 500 ms, which remove the impurities effectively, such as Ca, Na, Mg et al. Moreover, profit from that, the graphitization and layer spacing have been effectively improved, thereby further enhancing the electrochemical properties. Applied in the LIBs, the FWG anode exhibited an excellent reversible capacity with 413 mAh/g at 0.5C. Even at 2.0C, it still shows a capacity retention of 90.1 % after 1000cycles. That has certain advantages compared with other graphite materials. In addition, compared with the traditional recycling method, this direct regeneration method has the advantages of non-pollution and low energy consumption, and truly realizes the green, low-cost and high-value utilization of photovoltaic waste.

2. Experimental Section

2.1. The upcycling of photovoltaic waste graphite

The waste graphite comes from the waste heater of single crystal furnace. The bulk WG was initially crushed by a crusher, and then ground by a high-energy ball mill at 800 r/min for 6 h, and then sieved with 200 mesh for use. Weighting 200 mg of waste graphite into a quartz tube placed in the FJH device, the two ends of the graphite plug tightly pressed to adjust the resistance of the system in the 1.5–2 Ω, keep the vacuum state to regulate the pulse voltage of 200 V, observed "flash" phenomenon, cooled down and labeled as FWG. In addition, the waste graphite was treated in mixed acid for 2 h as a control experiment and labeled as LWG.

2.2. Characterization methods

Analysising the physical phases and crystal structures of the samples by X-ray diffraction (XRD, TDXRD) at 10–90°. The carbon content was analyzed by Thermogravimetric analyzer (TG, STA6000) at a heating rate of 10 ℃/min to 1000 ℃. The Inductively Coupled Plasma Emission Spectrometer (ICP-OES, Agilent 725-ES) was used by analyze the impurities content of the material; Raman spectroscopy (Labrm hr evolution) was used to analyze the degree of graphitization; Scanning Electron Microscopy (SEM, Hitanchi S-4800) and Transmission Electron Microscopy (TEM, Fei-Talos-F200X) were used to analyze the microscopic morphology; X-ray Photoelectron Spectroscopy (XPS, Thermo Escalab 250XI) was used to analyze the elemental composition of the material surfaces; Electron Paramagnetic Resonance (EPR, Bruke Emx) was used to analyze the electron vacancies.

2.3. Electrochemical measurement

Utilizing the CR2032 coin cell to study the electrochemical properties of upcycling graphite. In accordance with a mass ratio of 8:1:1, the active materials of WG, LWG, FWG and commercial graphite (CG), conductive carbon (Super-P,Timcal) and polyvinylidene fluoride (PVDF, ≥99.5 %, Aladdin) were stirred in the solvent of *N*-methyl-2-pyrrolidone (NMP, ≥99.5 %, Aladdin) for 12 h, and then coated on a copper foil collector and vacuum-dried for 8 h at 100 ℃. Using the lithium foils as the anode, glass microfiber filter (Whatman GF/D, Cytiva) as the diaphragm, 1 M $LiPF_6$ as the electrolyte, and a 2032-type coin cell was assembled in glove box with an argon atmosphere. The full cell was assembled according to the N/P ratio of 1.1. The commercial lithium iron phosphate ($LiFePO_4$), Super-P and PVDF were mixed in the NMP with a mass ratio of 8:1:1, and then coated uniformly on the aluminum foil as the cathode. The WG and FWG electrode were pre-lithiation in the half cell as the anode. Then, it was assembled in a glove box. After that, over a voltage range of 2.4 to 4.0 V, there is a test of the full cells electrochemical performance. Electrochemical charge/discharge measurements were tested on the NEWARE (CT4008) equipment at different current density less than 3.0 V voltage range. Princeton electrochemical workstation was performed to test the cyclic voltammetry (CV) at different scan rate and the electrochemical impedance spectroscopy (EIS).

3. Results and discussion

The details of FJH process are shown in Fig. 1a–d. Generally, the photovoltaic waste graphite mainly made up of the lumps (Fig. S1). It

needs to be milled into micrometer-sized powders via crushing and ball milling before the FJH process. Then, weighed a certain amount of waste graphite powder and filled into a quartz tube reaction vessel. Through adjusting the distance between two graphite plug spacers to control the electric resistance of system at ~2 Ω. Setting the reaction voltage parameter to 200 V, the current reached ~226 A less 500 ms (Fig. 1c). With the speedily heating rates (~ 8.3 × 10^5 k/s) and cooling rates (~ 4 × 10^3 k/s), the peak temperature reached ~ 3500 K via the infrared temperature sensor. By the way, the whole upcycling process must keep an inert atmosphere refrain from high-temperature oxidation of graphite materials.

The fast heating and cooling in seconds began to materialize via FJH [20,21], much less than those reported of traditional heat treatment and graphitization methods (Fig. 2a) [12,22–27]. Promising to realize the green and efficient recycle of solid waste. Meanwhile, exploring the effects of voltage and time for performance in Fig. 2b. As the flash voltage increases from 100 to 200 V and the reaction time increases from 50 to 500 ms, the temperature and graphitization degree are increasing, better result achieved at 200 V, 500 ms (Fig. S2).

Characterizing the structural characteristics by the XRD. As illustrated in Fig. 2c, all samples occur a strong and sharp diffraction peak at 26.5°, which corresponds to typical 2H graphite phase (JCPDS No. 41–1487). The peak of (002) migrate slightly to a small angle after FJH from 26.49° (WG) to 26.43°(FWG). This shift in the angle of the diffraction peak is usually associated with increased layer spacing [28]. In addition, the weak peak of all samples at 35.68° belong to the (111) crystal plane of SiC that originate in the reaction of the silicon vapor and carbon during the pulling process of monocrystalline silicon [29]. The XRD result of ash also further illustrates that the impurity is consist of the SiC (Fig. S3). Base on the features of corrosion resistance and high temperature resistance, the SiC is not easy to remove via leaching and heating treatment [30].

The Raman spectroscopy was used to analyze the feature changes during the FJH in Fig. 2d. Observing that the characteristic peaks at 1358, 1570 and 2700 cm^{-1} correspond to the D, G and 2D band. The D peak reflects the degree of defects and structural irregularities. And the G peak represents the in-plane stretching of sp^2 hybridized carbon, its intensity reflects the orderliness of the crystalline material [31]. In general, ID/IG is commonly used to characterize the graphitization degree of carbon materials. The ID/IG values of WG, LWG, and FWG are 0.53, 0.47, and 0.14, respectively. The ID/IG value of FWG is comparable to the commercial graphite (CG) (Fig. S4), which demonstrates that the FJH process could enhance the graphitization degree [15].

In addition, studying the variation in carbon content and metal impurities by the TG and ICP-OES. Comparing the TG curves of all materials (Fig. S5), the weightless temperature is mainly concentrated in 700–1000 ℃. The mass loss rate reached 96.09 %, 97.6 % and 98.55 % of WG, LWG and FWG eventually, suggestes that there is an increase in carbon content after FJH. Furthermore, the content of micro impurity is analyzed via the ICP-OES (Fig. 2e). The WG mainly contains with Ca, Fe, Al and Mg elements et al. These impurities can gasification off under the high-temperature effectively, and the content of impurities decreases to

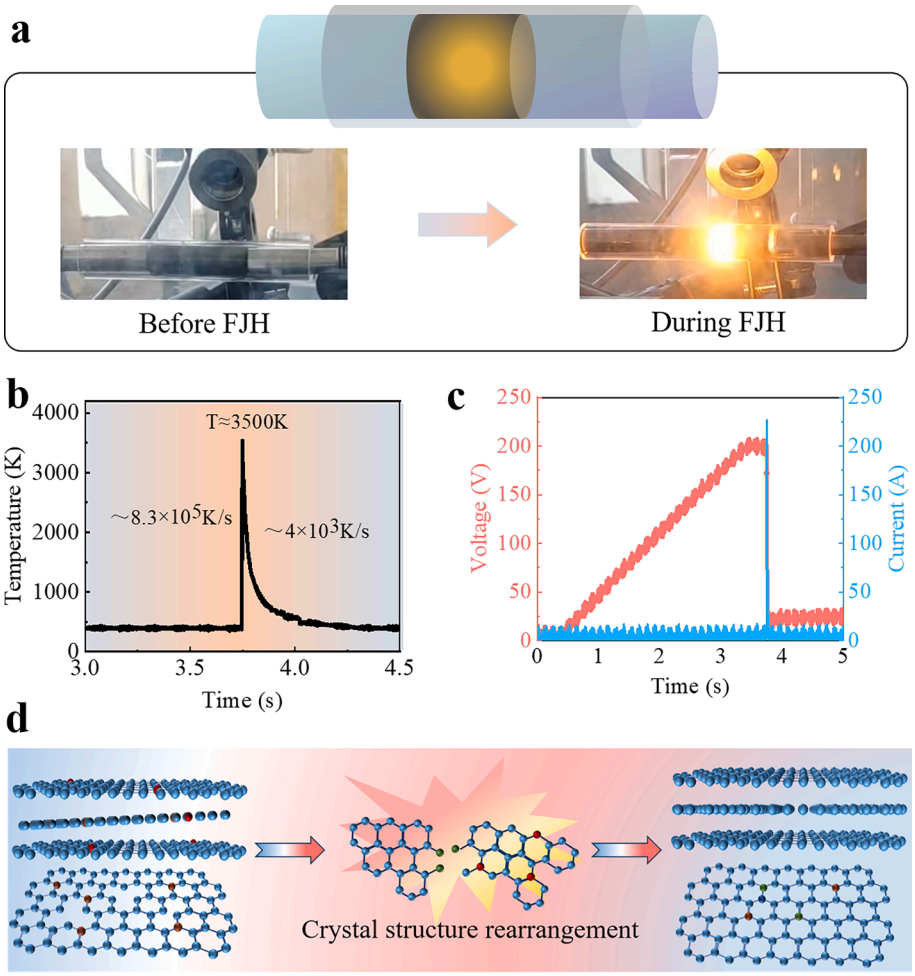

Fig. 1. Upcycling photovoltaic waste graphite by flash joule heating. a) Schematics of the synthesis of photovoltaic waste graphite via flash joule heating. b) The enlarged images of real Time-Temperature measurement during the FJH process. c) The real Time-Voltage and Time-Current measurement during the FJH process. d) The upcycling mechanism schematic illustrations of the WG during the FJH.

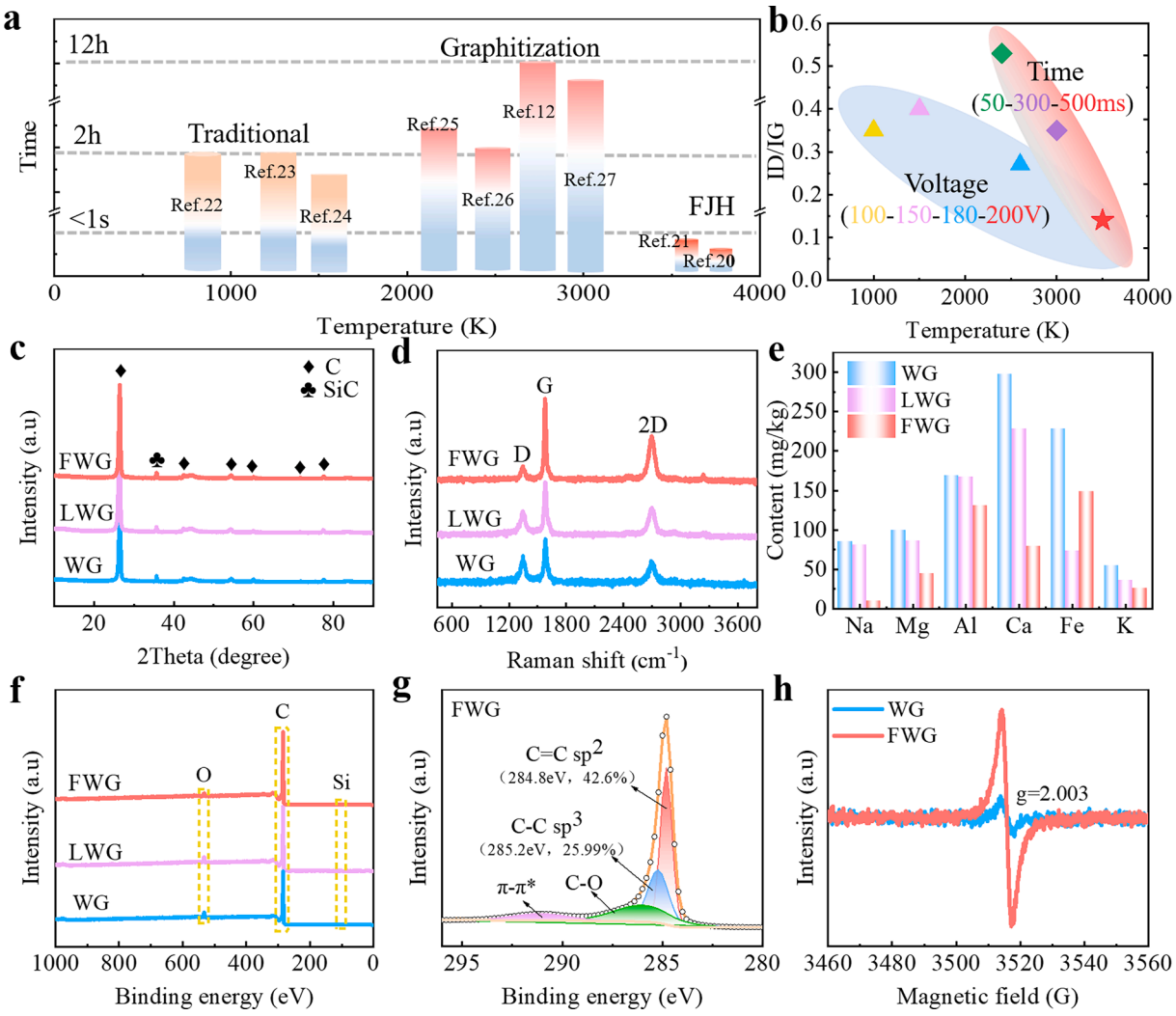

Fig. 2. Structural and compositional characterization of the samples. a) Comparison of the time–temperature of the FJH with traditional heating and graphitization. b) ID/IG value of upcycling graphite under different FJH process. c) XRD patterns. d) Raman spectra. e) ICP-OES. f) XPS survey spectra. g) The high-resolution spectra of C 1 s of FWG. h) EPR spectra of WG and FWG.

< 150 ppm. Comparing to the leaching, FJH can effectively remove impurities. The reason of that can be elucidated as follows: On the one hand, the isostatic pressure preparation makes the residual impurities closely encapsulated with the graphite material, which is not easy to be removed in acid leaching. On the other hand, graphite has good thermal conductivity, which enables effective heat transfer to vaporize the impurities and remove them.

The chemical composition and changes of the elements were employed to analyze via XPS in Fig. 2f–g. All samples exihibit the C 1 s, O 1 s and a weaker Si 2p peaks in Fig. 2f. It is consistent with the results of XRD. The high-resolution plot of C1s of FWG material shown in Fig. 2g, which splits into four peaks of C═C sp^2, C—C sp^3,C—O and π-π* bonds at 284.8, 285.2, 286.0 and 291.01 eV. FWG mainly consists of sp^2 and sp^3, that represent graphitic-carbon structures and a partial defect in the graphite structure separately [32]. Meanwhile, the content of the sp^2 / sp^3 are 42.6 %/25.99 %, much better than the WG (37.61 %/31.24 %) and LWG (38.26 %/28.17 %) (Fig. S6), indicates that the FJH processes can reconstruct graphite structure and reduce the defects. The Fig. S6 shows the high-resolution O 1 s spectrum with two peaks located at 532.1 eV and 533.1 eV, corresponding to C═O and C—O bonds respectively. The reduction in the intensity of C═O may be related to the removal of oxygen-containing groups. Furthermore, the decrease of the oxygen percentage to FWG is also illustrated that. (Table S1).

The EPR was studied to explore the structural features. Observed a strong resonant signal at g = 2.003 of WG and FWG in Fig. 2h, these signals are assigned to the oxygen vacancy. Owing to the oxygen-containing impurities evaporate under the high-temperature, FWG has stronger signal strength than WG. The presence of these oxygen vacancies provides additional active sites to enhanced lithium-ion transfer between graphite sheet layers [33].

Then, the morphology characterization is revealed by the SEM (Fig. S7a–c). The WG is mainly made of irregular flakes, and tight stacking between layers owing to the special isostatic pressure treatment. That is not conducive to the application for anode materials. After leaching, it still exists as stacked flakes while almost no change in morphology. Under the rapidly ultra-high temperature treatment, the waste graphite flake layer has undergone obvious exfoliation, and the distribution of flakes is more dispersed and uniform. Then, the morphology and structure features are revealed by the TEM and high-resolution transmission electron micrograph (HRTEM) in Fig. 3a–j. The multilayered stack of WG exhibits the lattice stripe of discontinuous and numerous of defects by its corresponding inverse Fast Fourier Transformation (IFFT) images (Fig. 3d). During the fast high-temperature upcycle, the lattice stripe of FWG transform to regular and ordered gradually just as the schematic illustration of the morphology transformation (Fig. 3j). Meanwhile, the spacing also

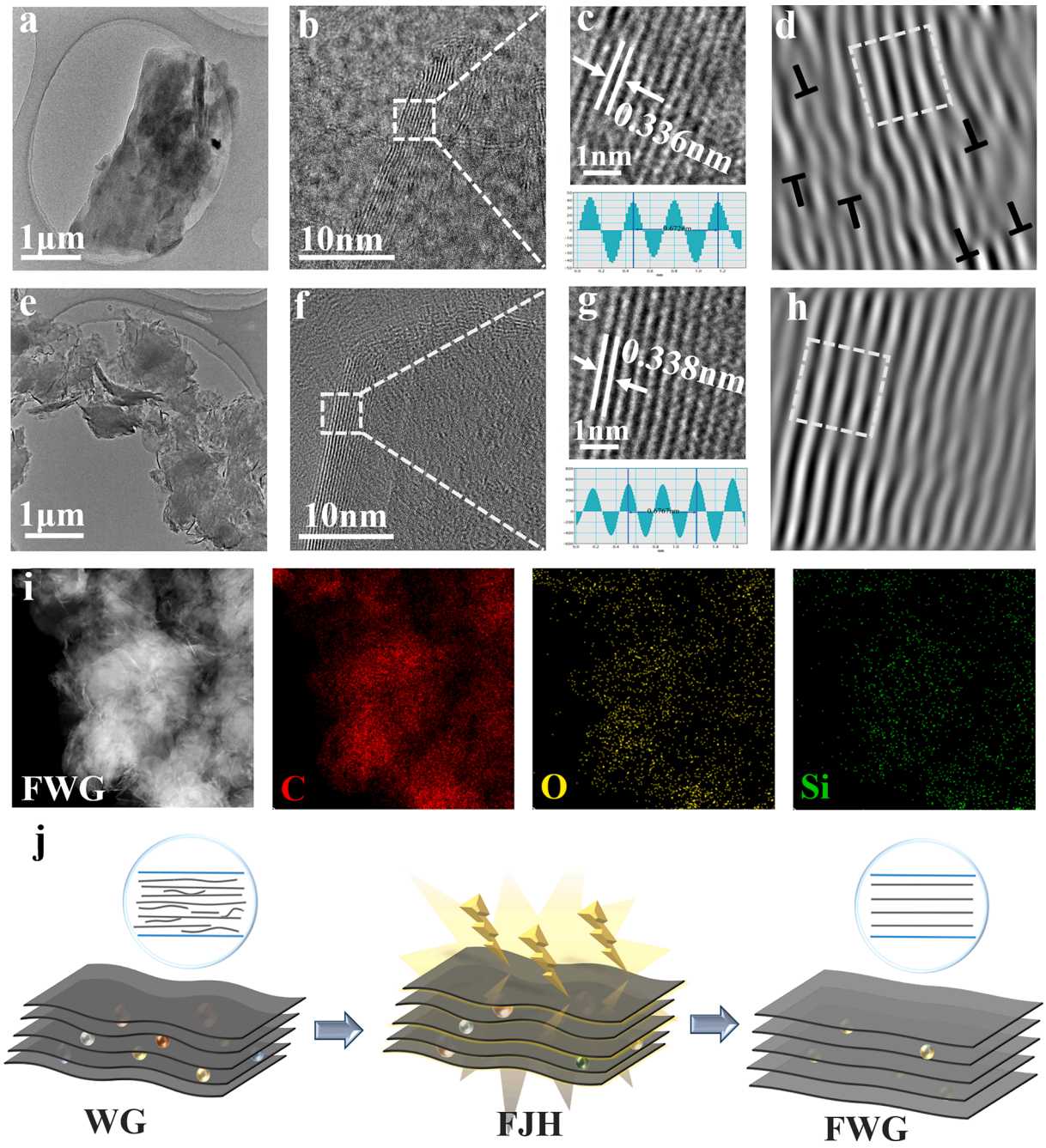

Fig. 3. The morphology of the WG and FWG. a, e) TEM of WG and FWG. b, f) HRTEM diagram of WG and FWG. c, g) The interlayer spacings of WG and FWG. d, h) The IFFT diagram of WG and FWG. i) The EDS mappings of FWG. j) Schematic illustration of the morphology transformation during the FJH process.

increased from 0.336 nm (WG) to 0.338 nm (FWG) (Fig. 3g), which could facilitate the Li^+ diffusion rate, thereby enhancing the fast-charging performance of graphite anode. The elements of WG, LWG and FWG mainly contained C, Si and O, and the element distribution was uniform (Fig. S8). After FJH process, the content of the C elements is increased, corresponding to the above results (Table S2).

Further investigation of the implications of the electrochemical characterization after FJH of waste graphite, tested a series of electrochemical characterizations. The initial galvanostatic charge–discharge (GCD) curves show in Fig. 4a at 0.5C of all samples. The initial discharge capacity of FWG is 648 mAh/g while that the CG is 466 mAh/g, the enlarged capacity originates from the enlarged layer spacing and the formation of oxygen vacancies in FWG, which provide more active sites for Li^+. In addition, the GCD curves of WG, LWG and FWG show smaller slopes when the voltage exceeds 0.3 V comparing to commercial graphite, which manifest that exist the different Li^+ storage mechanism [34]. Furthermore, founding a small voltage plateau at 0.8 V that may be related to the lithium intercalation of silicon carbide [17]. Theoretically, SiC is an electrochemical inertia material. It was found that high-temperature graphitization treatment of SiC surface can improve its lithium storage properties recently [35,36]. After "activating", Li^+ will occupy the (1/4, 1/4, 1/4) and (1/2, 1/2, 1/2) interstitial sites during the lithium deintercalation process to form Li_xSiC. With the increased intercalation of Li^+ to 12, the Li_xSiC will form Li_2SiC and its specific capacity reaches 1336 mAh/g [37,38]. That provides more specific capacity for the FWG anode. Besides, study the charge–discharge performance of the FWG anode with different cycle number at 1.0C (Fig. 4b). The initial charge–discharge capacity is 403 mAh/g/603 mAh/g. With

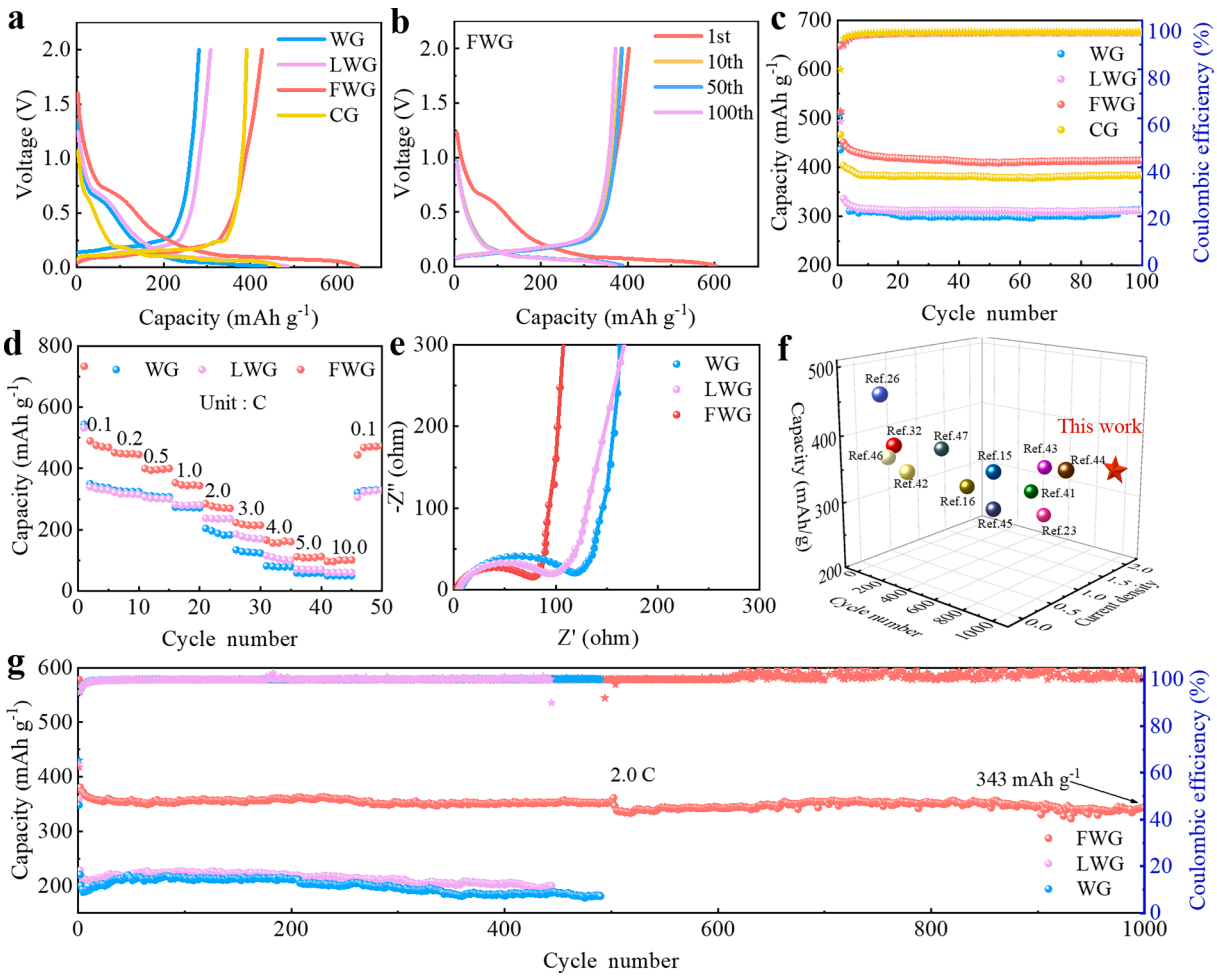

Fig. 4. Electrochemical performance of the all samples. a) The initial charge–discharge profiles of WG, LWG, FWG and CG at 0.5C. b) The different cycles of charge–discharge profiles by the FWG at 1.0C. c) The cycling performance of WG, LWG, FWG and CG electrodes at 0.5C. d) Rate performance of WG, LWG and FWG electrode. e) Nyquist plots of WG, LWG and FWG electrode. f) Comparison of the capacity of the FWG electrode with those of previously reported graphite-based anodes. g) Long-term cycling performance of WG, LWG, and FWG.

the increase in the number of cycles, the charge–discharge curves almost coincident, which further indicates that the FWG anode has excellent reversibility. Up to the 200th cycle, the FWG anode maintains a high capacity of 397.4mAh/g, corresponds to the 94.1 % capacity retention rate. (Fig. S9).

Fig. 4c shows the cycling performance at 0.5C of WG, LWG, FWG and CG. After 100cycles, FWG anode still maintains 413 mAh/g that much higher than WG (308 mAh/g) and LWG (312 mAh/g). Among them, found that the slight change for the capacity performance after leaching, that attributed to the leaching is not effectively realizing the structural improvements [39]. Then, the rate performance was further evaluated from 0.1C to 10.0C in Fig. 4d. The FWG demonstrates an outstanding rate performance, it showed a specific capacity of 471 mAh/g at 0.1C. Even at a large current of 10.0C, its capacity obviously better than those of WG and LWG. When the current returned to 0.1C, the capacity still recovered the initial capacity.

The electrochemical properties of the upcycling graphite anodes were investigated by electrochemical impedance spectroscopy (EIS). In Fig. 4e, all samples composed of semicircles and straight lines. In general, the diameters of the semicircles in the high-frequency region represent the charge transfer resistance (R_{ct}), and the straight lines in the low-frequency region reflect the Warburg impedance associated with Li^+ diffusion throughout the electrode [40]. Fitting by the equivalent circuit model, the FWG showed enhanced charge and ion transport abilities, its display a lower charge transfer resistance (Rct = 64.08 Ω) while that the WG is 99.16 Ω, indicates that the FWG exhibit the more quickly Li^+ transfer ability.

The long-term cycling test was performed on Fig. 4g. The FWG demonstrated an outstanding cycling property than WG and LWG, its initial reversible capacity reached 578mAh/g at 2.0C. It still retained 343 mAh/g, the capacity retention reaches 90.1 % after 1000cycles. Comparing with previous literature (Fig. 4f), the FWG still display superior electrochemical properties for these recycle graphite anode (Table S3) [15,23,26,32,41–48] and commercial graphite (Fig. S10). This upcycling PV waste graphite is promising alternative to battery-grade graphite.

To further explore electrochemical reaction kinetics of upcycling graphite, the CV tests were performed with the different scanning rate of 0.1–1.0 mV/s (Fig. 5a–b). During the first scan process, observing that the reduction peak near the 1.2 V, which is inclined towards the generation of SEI. To further explore its charge storage mechanism, the relative connection between sweep rate (v) and current (i) are calculated by the following formulas:

$$i = av^b$$

Taking the logarithm of both side:

$$\log i = \log a + b \log v$$

where *i* and *v* represent the applied current intensity and the scan rate at

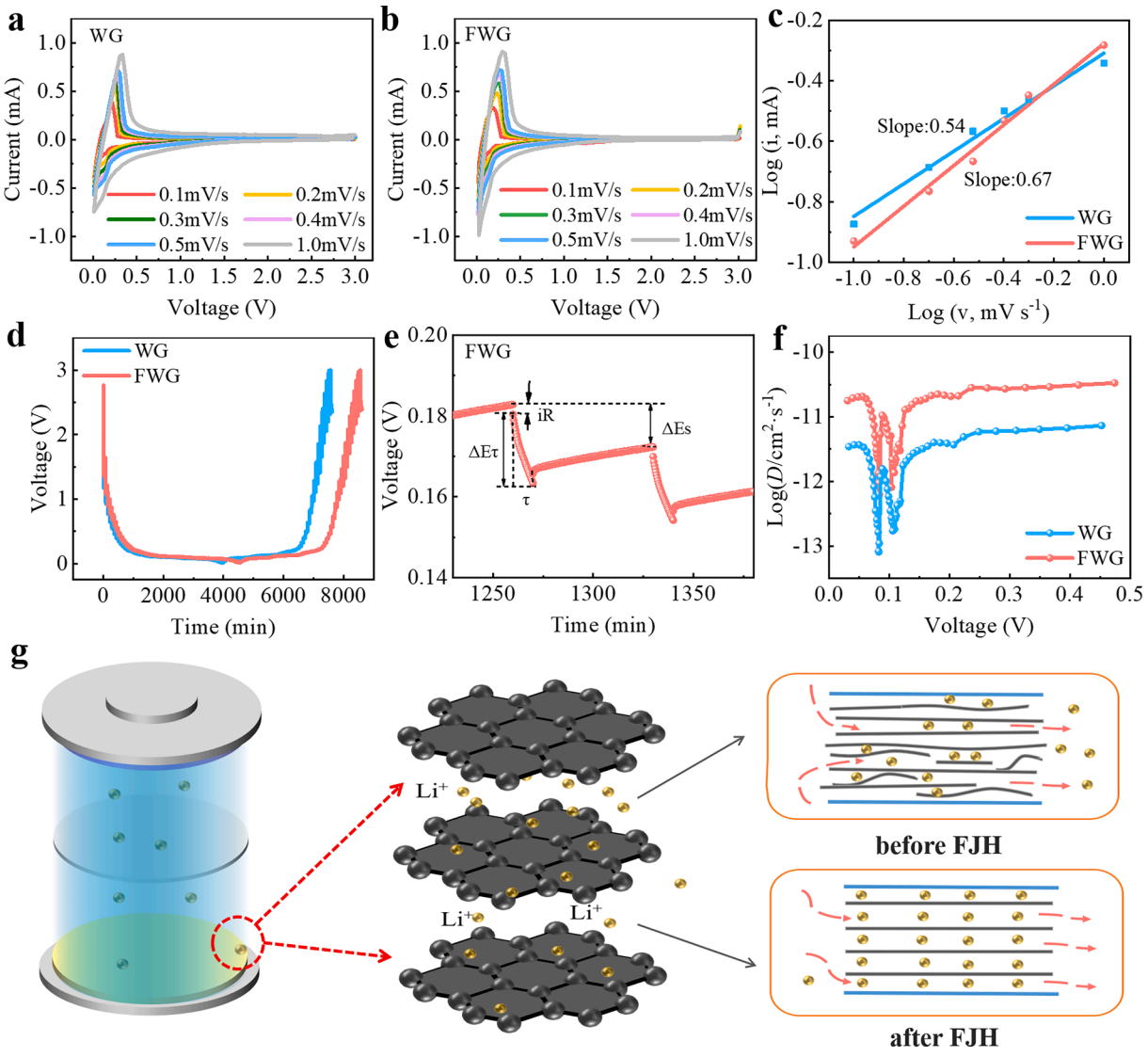

Fig. 5. Electrochemical kinetics analysis of WG and FWG. a, b) CV curves at different scan rate of 0.1–1 mV/s. c) Linear plot between log(i) and log(v) for the reduction peaks. d) The voltage profiles versus degree of lithiation of GITT. e) The zoomed-in voltage versus time curve from the GITT measurement. f) Lithium-ion diffusion coefficient from the GITT measurement. g) Schematic diagram of lithium-ion diffusion.

different voltages, *a* and *b* represent the fitting parameters [49].

Theoretically, the b-value reflects the lithium storage mechanism of pseudocapacitive reactions or diffusion control. When b = 0.5 means that the capacity is controlled by diffusion, and b = 1 means that controlled by pseudocapacitive [50]. In Fig. 5c, the fitting parameter b value of FWG reach 0.67, which indicating that the lithium-ion transport mechanism is dominated by diffusion control and pseudocapacitance. Benefit from the structural advantagesthe of regular and ordered, the Li^+ diffusion rate on the graphite surface of the FWG gaines effective improvement.

Furthermore, the diffusion coefficient of lithium ions was calculated by the galvanostatic intermittent titration technique (Fig. 5d–f). Compared to WG, FWG own a lower irinternal (iR, 0.0024 V) (Fig. S11), which indicate that the upcycling graphite process good conductivity (Fig.S11), which indicate that the upcycling graphite process good conductivity [51]. Supposing that the diffusion of lithium ions within both WG and FWG obeys Fick's second law of diffusion, the Li^+ diffusion coefficient (D_{Li^+}) can be calculated by the following equation:

$$D_{Li^+} = \frac{4}{\tau\pi}\left(\frac{m_B V_M}{M_B S}\right)^2\left(\frac{\Delta E_S}{\Delta E_\tau}\right)^2$$

where V_M, m_B and M_B are the molar volume, the active material mass and the molecular mass respectively, and τ is relaxation time, s is the contact area of the electrode / electrolyte; ΔE_S is the steady-state potential change in τ time after applying a constant current, and ΔE_τ is the voltage change during the galvanostatic discharge and charge [52].

The Li^+ diffusion coefficients of WG and FWG display a trend of decrease-increase–decrease-increase with the embedding of Li^+ in a "W"-shaped curve in Fig. 5f, which is associated with the displacement of the phase transition during interlayer diffusion. The values of D_{Li}^+ of FWG range from $8.3 \times 10^{-14} - 2.49 \times 10^{-10}$, which higher 1–2 orders of magnitude than that of the WG and LWG (Fig. S12), suggests that the regularly ordered structure is more favorable to improve the lithiation kinetics (Fig. 5g). Meanwhile, the Li^+ diffusion coefficients were mainly distributed at 10^{-11} cm^2/s, revels that the samples showed fast and uniform Li^+ diffusion at different voltages, which exhibited good electrochemical performance.

The FWG display excellent capacity and cycling stability. To further verify the possibility of the FWG material for practical applications, it performed a full battery test. The schematic diagram of the full cell is shown in Fig. 6a. Among them, the commercial $LiFePO_4$ was used as the cathode and the FWG (or WG) was used as the anode. Notably, the FWG

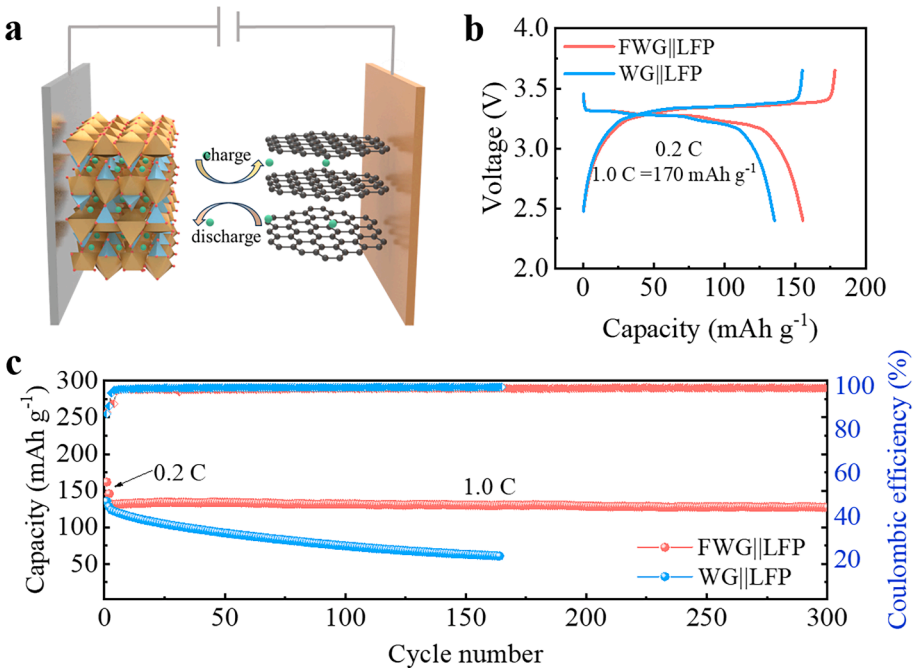

Fig. 6. The electrochemical performance of the full cell. a) Schematic illustration of the full-cell. b) The initial charge–discharge curves of the WG||LFP and FWG||LFP full-cell at 0.2C. c) The cycling performance of WG||LFP and FWG||LFP full-cell at 1.0C.

and WG anodes need to achieve pre-lithiation in the half-cell. There are the GCD curves of the full-cell in Fig. 6b. During the voltage range of 2.4—4.0 V, the initial specific capacity of WG||LFP is 135 mAh/g, and the FWG||LFP capacity is 161 mAh/g corresponding to the initial coulombic efficiency is 88.1 %. After 300 cycles, the FWG||LFP still shows a capacity retention of 78.8 % while that the WG||LFP is dropping dramatically, indicating that the FWG||LFP has good electrochemical stability. In summary, the FWG electrode is promising to be applied successfully in the field of high-energy–density LIBs.

4. Conclusion

In conclusion, the upcycling of photovoltaic waste graphite into high performance graphite anode realizes by flash Joule heating effectively. After rapid heating, the impurity content was reduced from 3.91 % to 1.45 %. The ID/IG value was reduced from 0.53 to 0.14, which effectively improved its graphitization degree. Meanwhile, the enlarged layer spacing from 0.336 to 0.338 nm provide more active sites for the intercalation and deintercalation of Li^+. Consequently, FWG maintains an outstanding capacity of 343 mAh/g at 2.0C with a capacity retention of 90.1 % after 1000cycles. Even at a large current of 10.0C, it still much better than the WG and LWG. The excellent electrochemical properties and green and efficient regeneration of FWG provide an emerging pathway for the value-added recycling of PV waste graphite. However, the lower initial coulombic efficiency restricts its development, and how to improve will be the key to the commercial application of PV waste graphite.

CRediT authorship contribution statement

Jianjiao Xiong: Writing – original draft, Software, Resources, Methodology, Investigation, Data curation. **Yanfeng Wang:** Software, Methodology, Investigation, Data curation. **Jijun Lu:** Writing – review & editing, Methodology, Investigation, Formal analysis. **Fengshuo Xi:** Supervision, Resources, Formal analysis. **Zhongqiu Tong:** Software, Resources, Investigation. **Wenhui Ma:** Project administration, Methodology, Funding acquisition. **Shaoyuan Li:** Writing – review & editing, Resources, Methodology, Funding acquisition.

Declaration of competing interest

The authors declare that they have no known competing financial interests or personal relationships that could have appeared to influence the work reported in this paper.

Acknowledgements

This work were supported by the National Natural Science Foundation of China (Grant No. 22468029, 52274408, 52204314), Major Science and Technology Projects in Yunnan Province (No. 202402AF080005), Yunnan Fundamental Research Projects (202201AW070014), and the Program for Innovative Research Team in University of Ministry of Education of China (No. IRT_17R48).

Appendix A. Supplementary data

Supplementary data to this article can be found online at https://doi.org/10.1016/j.jcis.2025.01.175.

Appendix C. Supplementary data

Supplementary data to this article can be found online at https://doi.org/10.1016/j.jcis.2025.01.175.

Data availability

No data was used for the research described in the article.

References

[1] Y. Yu, S. Li, F. Xi, H. Lan, D. Wu, Z. Chen, W. Ma, R. Deng, Influence of the structural differences between end-of-life Al-BSF and PERC modules on the Al leaching separation behavior, Sol. Energy 263 (2023) 111938, https://doi.org/10.1016/j.solener.2023.111938.

[2] P. Li, Y. Sun, Z. Hu, S. Li, J. Li, Y. Tan, Comprehensive recycling and utilization of photovoltaic waste: Use photovoltaic glass waste to refine silicon kerf waste, Sep. purif.technol. 317 (2023) 123863, https://doi.org/10.1016/j.seppur.2023.123863.

[3] C. Breyer, D. Bogdanov, A. Aghahosseini, A. Gulagi, M. Child, A.S. Oyewo, J. Farfan, K. Sadovskaia, P. Vainikka, Solar photovoltaics demand for the global energy transition in the power sector, Prog.photovoltaics. 26 (8) (2018) 505–523, https://doi.org/10.1002/pip.2950.
[4] J. Guo, X. Liu, J. Yu, C. Xu, Y. Wu, D.A. Pan, R.A. Senthil, An overview of the comprehensive utilization of silicon-based solid waste related to PV industry, Resour.conserv.recyc. 169 (2021) 105450, https://doi.org/10.1016/j.resconrec.2021.105450.
[5] L. Zhong, L. Guo, J. Wang, Q. Song, H. Li, Y. Li, Excellent heat transfer and mechanical properties of graphite material with rolled-up graphene layers, Carbon 208 (2023) 123–130, https://doi.org/10.1016/j.carbon.2023.03.041.
[6] Y. Hu, Z. Chen, Y. Zhang, X. Chen, W. Ma, SiC Generation Mechanism in Photovoltaic Crystal Pulling Waste Graphite Infusion Cylinder, SILICON 16 (7) (2024) 3141–3153, https://doi.org/10.1007/s12633-024-02888-y.
[7] P. Jia, J. Sun, S. Li, W. Wang, Z. Song, X. Zhao, Y. Mao, A feasible recycling route for spent graphite: Microwave-assisted puffing with Fe2O3 loading to construct high-performance anode for lithium-ion batteries, Materials.today.sustain. 25 (2024) 100620, https://doi.org/10.1016/j.mtsust.2023.100620.
[8] L. Wang, J. Yu, S. Li, F. Xi, W. Ma, K. Wei, J. Lu, Z. Tong, B. Liu, B. Luo, Recent advances in interface engineering of silicon anodes for enhanced lithium-ion battery performance, Energy.storage.mater. 66 (2024) 103243, https://doi.org/10.1016/j.ensm.2024.103243.
[9] H. Zhang, Y. Yang, D. Ren, L. Wang, X. He, Graphite as anode materials: Fundamental mechanism, recent progress and advances, Energy.storage.mater. 36 (2021) 147–170, https://doi.org/10.1016/j.ensm.2020.12.027.
[10] Z. Shang, W. Yu, J. Zhou, X. Zhou, Z. Zeng, R. Tursun, X. Liu, S. Xu, Recycling of spent lithium-ion batteries in view of graphite recovery: A review, eTransportation. 20 (2024).doi: 10.1016/j.etran.2024.100320.
[11] X. Bu, Z. Tong, M. Bilal, X. Ren, M. Ni, C. Ni, G. Xie, Effect of ultrasound power on HCl leaching kinetics of impurity removal of aphanitic graphite, Ultrason. sonochem. 95 (2023) 106415, https://doi.org/10.1016/j.ultsonch.2023.106415.
[12] G.-Q. Yu, M.-Z. Xie, Z.-H. Zheng, Z.-G. Wu, H.-L. Zhao, F.-Q. Liu, Efficiently regenerating spent lithium battery graphite anode materials through heat treatment processes for impurity dissipation and crystal structure repair, Resour. conserv.recyc. 199 (2023) 107267, https://doi.org/10.1016/j.resconrec.2023.107267.
[13] W. Yan, Z. Chen, S. Ma, S. Chen, Y. Lu, M. Wang, L. Chen, Q. Huang, B. Wang, Y. Su, J. Wang, N. Li, F. Wu, Unraveling the relationship between the mineralogical characteristics and lithium storage performance of natural graphite anode materials, Carbon 227 (2024) 119270, https://doi.org/10.1016/j.carbon.2024.119270.
[14] N. Flores Medina, M. del Mar Barbero-Barrera, F. Jové-Sandoval, Improvement of the mechanical and physical properties of cement pastes and mortars through the addition isostatic graphite, Constr.build.mater. 189 (2018) 898–905, https://doi.org/10.1016/j.conbuildmat.2018.09.055.
[15] S. Dong, Y. Song, K. Ye, J. Yan, G. Wang, K. Zhu, D. Cao, Ultra-fast, low-cost, and green regeneration of graphite anode using flash joule heating method, EcoMat 4 (5) (2022) e12212, https://doi.org/10.1002/eom2.12212.
[16] Z. Cheng, Z. Luo, H. Zhang, W. Zhang, W. Gao, Y. Zhang, L. Qie, Y. Yao, Y. Huang, K.K. Fu, Targeted regeneration and upcycling of spent graphite by defect-driven tin nucleation, Carbon Energy 6 (4) (2024) e395.
[17] C. Sun, X. Xu, C. Gui, F. Chen, Y. Wang, S. Chen, M. Shao, J. Wang, High-Quality Epitaxial N Doped Graphene on SiC with Tunable Interfacial Interactions via Electron/Ion Bridges for Stable Lithium-Ion Storage, Nano-Micro.lett. 15 (1) (2023) 202, https://doi.org/10.1007/s40820-023-01175-6.
[18] B. Deng, Z. Wang, W. Chen, J.T. Li, D.X. Luong, R.A. Carter, G. Gao, B.I. Yakobson, Y. Zhao, J.M. Tour, Phase controlled synthesis of transition metal carbide nanocrystals by ultrafast flash Joule heating, Nat.Commun. 13(1) (2022).doi: 10.1038/s41467-021-27878-1.
[19] K.M. Wyss, J.T. Li, P.A. Advincula, K.V. Bets, W. Chen, L. Eddy, K.J. Silva, J. L. Beckham, J. Chen, W. Meng, B. Deng, S. Nagarajaiah, B.I. Yakobson, J.M. Tour, Upcycling of Waste Plastic into Hybrid Carbon Nanomaterials, Adv.mater. 35 (16) (2023) 2209621, https://doi.org/10.1002/adma.202209621.
[20] Y. Liao, R. Zhu, W. Zhang, Z. Liu, H. Zhu, Y. Sun, Ultrafast synthesis of novel coal-based graphene and its anticorrosion properties of epoxy/graphene nanocomposite coatings, Prog.org.coat. 184 (2023) 107859, https://doi.org/10.1016/j.porgcoat.2023.107859.
[21] L. Wang, S. Zhu, Z. Huang, M. Li, Y. Zhao, G. Han, Y. Li, J. Ni, Rapid and Up-Scalable Flash Fabrication of Graphitic Carbon Nanocages for Robust Potassium Storage, Adv.funct.mater. 2401548 (2024) 2401548, https://doi.org/10.1002/adfm.202401548.
[22] J. Zhang, Y. Lei, Z. Lin, P. Xie, H. Lu, J. Xu, A novel approach to recovery of lithium element and production of holey graphene based on the lithiated graphite of spent lithium ion batteries, Chem.eng.j. 436 (2022) 135011, https://doi.org/10.1016/j.cej.2022.135011.
[23] Y. Dong, Z. Zeng, Z. Yuan, B. Wang, H. Lei, W. Zhao, W. Ai, L. Kong, Y. Yang, P. Ge, Spent graphite regeneration: Exploring diverse repairing manners with impurities-catalyzing effect towards high performance and low energy consumption, J.energy. chem. 91 (2024) 656–669, https://doi.org/10.1016/j.jechem.2023.12.052.
[24] K. Yang, P. Gong, Z. Tian, Y. Lai, J. Li, Recycling spent carbon cathode by a roasting method and its application in Li-ion batteries anodes, J.clean.prod. 261 (2020) 121090, https://doi.org/10.1016/j.jclepro.2020.121090.
[25] L. Tang, Q. Mao, Z. You, Z. Yao, X. Zhu, Q. Zhong, J. Xiao, Catalytic graphitization in anthracite by reduced iron particles and investigating the mechanism of catalytic transformation via molecular dynamics, Carbon 188 (2022) 336–348, https://doi.org/10.1016/j.carbon.2021.12.031.
[26] K. Yang, Z. Zhao, X. Xin, Z. Tian, K. Peng, Y. Lai, Graphitic carbon materials extracted from spent carbon cathode of aluminium reduction cell as anodes for lithium ion batteries: Converting the hazardous wastes into value-added materials, J.taiwan.inst.chem.e. 104 (2019) 201–209, https://doi.org/10.1016/j.jtice.2019.09.012.
[27] H. Yu, H. Dai, Y. Zhu, H. Hu, R. Zhao, B. Wu, D. Chen, Mechanistic insights into the lattice reconfiguration of the anode graphite recycled from spent high-power lithium-ion batteries, J.power.sources. 481 (2021) 229159, https://doi.org/10.1016/j.jpowsour.2020.229159.
[28] G. Singh, J. Lee, R. Bahadur, A. Karakoti, J. Yi, A. Vinu, Highly graphitized porous biocarbon nanosheets with tunable Micro-Meso interfaces and enhanced layer spacing for CO2 capture and LIBs, Chem.eng.j. 433 (2022) 134464, https://doi.org/10.1016/j.cej.2021.134464.
[29] Y. Cheng, J. Chen, B. Deng, W. Chen, K.J. Silva, L. Eddy, G. Wu, Y. Chen, B. Li, C. Kittrell, S. Xu, T. Si, A.A. Martí, B.I. Yakobson, Y. Zhao, J.M. Tour, Flash upcycling of waste glass fibre-reinforced plastics to silicon carbide, Nat.sustain. 7 (4) (2024) 452–462, https://doi.org/10.1038/s41893-024-01287-w.
[30] Y. Han, D. Zou, Y. Kang, Z. Zhong, W. Xing, One-step sintering process for high-performance SiC membranes for efficient filtration of dust-laden gas, J.membrane. sci. 692 (2024) 122265, https://doi.org/10.1016/j.memsci.2023.122265.
[31] J. Xiong, Z. Yang, R. Zhou, A. Xiao, X. Kong, J. Jiang, L. Dong, Q. Zhuang, Z. Ju, Y. Chen, In Situ Defect Engineering in Carbon by Atomic Self-Activation to Boost the Accessible Low-Voltage Insertion for Advanced Potassium-Ion Full-Cells, Small 20 (27) (2024) 2402037, https://doi.org/10.1002/smll.202402037.
[32] S. Xie, Y. Dong, X. Wang, Z. Zeng, H. Zhou, Z. Yuan, W. Sun, X. Ji, Y. Yang, P. Ge, Tailored anion radii of molten-salts systems toward graphite regeneration with excellent energy-storage properties, Energy.storage.mater. 70 (2024) 103510, https://doi.org/10.1016/j.ensm.2024.103510.
[33] B. Sun, L. Kuang, G. Li, S. Yang, D. Zhang, C. Zhang, Q. Zhang, S. Ni, Synergistic structure and oxygen-vacancies engineering of lithium vanadate for kinetically accelerated and pseudocapacitance-dominated lithium storage, Chem.eng.j. 484 (2024) 149609, https://doi.org/10.1016/j.cej.2024.149609.
[34] S. Dong, Y. Song, M. Su, G. Wang, Y. Gao, K. Zhu, D. Cao, Flash Joule heating induced highly defective graphene towards ultrahigh lithium ion storage, Chem. eng.j. 481 (2024) 147988, https://doi.org/10.1016/j.cej.2023.147988.
[35] A.L. Lipson, S. Chattopadhyay, H.J. Karmel, T.T. Fister, J.D. Emery, V.P. Dravid, M. M. Thackeray, P.A. Fenter, M.J. Bedzyk, M.C. Hersam, Enhanced Lithiation of Doped 6H Silicon Carbide (0001) via High Temperature Vacuum Growth of Epitaxial Graphene, J.phys.chem.c. 116 (39) (2012) 20949–20957, https://doi.org/10.1021/jp307220y.
[36] H. Yu, X. Chen, H. Zhang, X. Xu, X. Hu, Z. Wang, J. Wang, S. Zhuang, M. Jiang, Large Energy Pulse Generation Modulated by Graphene Epitaxially Grown on Silicon Carbide, ACS Nano 4 (12) (2010) 7582–7586, https://doi.org/10.1021/nn102280m.
[37] S.H. Lee, C. Park, K. Do, H. Ahn, Maximizing the utilization of active sites through the formation of native nanovoids of silicon oxycarbide as anode materials in lithium-ion batteries, Energy.storage.mater. 35 (2021) 130–141, https://doi.org/10.1016/j.ensm.2020.11.018.
[38] R. Nandan, N. Takamori, K. Higashimine, R. Badam, N. Matsumi, Confronting the Issues Associated with the Practical Implementation of Zinc Blende-type SiC Anodes for Efficient and Reversible Storage of Lithium Ions, ACS.Appl.Energy. Mater. 7(6) (2024) 2088-2100.doi: 10.1021/acsaem.3c02676.
[39] Y. Weng, G. Chen, F. Dou, X. Zhuang, Q. Wang, M. Lu, L. Shi, D. Zhang, In situ growth of silicon carbide interface enhances the long life and high power of the mulberry-like Si-based anode for lithium-ion batteries, J.energy.storage. 32 (2020) 101856, https://doi.org/10.1016/j.est.2020.101856.
[40] K. Sun, X. Li, Z. Zhang, K. Fu, X. Xiao, L. Gong, P. Tan, Unexpected stable cycling performance at low temperatures of Li-ion batteries with Si/C anodes, Energy. storage.mater. 66 (2024) 103216, https://doi.org/10.1016/j.ensm.2024.103216.
[41] T. Li, L. Tao, L. Xu, T. Meng, B.C. Clifford, S. Li, X. Zhao, J. Rao, F. Lin, L. Hu, Direct and Rapid High-Temperature Upcycling of Degraded Graphite, Adv.funct.mater. 33 (43) (2023) 2302951, https://doi.org/10.1002/adfm.202302951.
[42] Z. Yuan, Y. Dong, Z. Zeng, W. Zhao, B. Wang, H. Lei, W. Sun, X. Ji, Y. Yang, P. Ge, For regenerated graphite: Tailoring sub-surface architecture with strong pre-storage abilities towards high-rate properties, Chem.eng.j. 491 (2024) 151948, https://doi.org/10.1016/j.cej.2024.151948.
[43] H. Da, S. Pan, J. Li, J. Huang, X. Yuan, H. Dong, J. Liu, H. Zhang, Greatly recovered electrochemical performances of regenerated graphite anode enabled by an artificial PMMA solid electrolyte interphase layer, Energy.storage.mater. 56 (2023) 457–467, https://doi.org/10.1016/j.ensm.2023.01.038.
[44] J. Luo, J. Zhang, Z. Guo, Z. Liu, S. Dou, W.-D. Liu, Y. Chen, W. Hu, Recycle spent graphite to defect-engineered, high-power graphite anode, Nano.res. 16 (4) (2023) 4240–4245, https://doi.org/10.1007/s12274-022-5244-z.
[45] H. Gong, H. Xiao, L. Ye, X. Ou, High-performance expanded graphite regenerated from spent lithium-ion batteries by integrated oxidation and purification method, Waste, Manage 171 (2023) 292–302, https://doi.org/10.1016/j.wasman.2023.08.046.
[46] Y.E.J. Lai, X. Zhu, J. Li, Q. Gou, M. Li, A. Xia, Y. Huang, X. Zhu, Q. Liao, Recovery and regeneration of anode graphite from spent lithium-ion batteries through deep eutectic solvent treatment: Structural characteristics, electrochemical performance and regeneration mechanism, Chem. Eng. J. 457 (2023) 141196, https://doi.org/10.1016/j.cej.2022.141196.
[47] D. Yang, Y. Yang, H. Du, Y. Ji, M. Ma, Y. Pan, X. Qi, Q. Sun, K. Shi, L. Qie, An efficient recycling strategy to eliminate the residual “impurities” while heal the damaged structure of spent graphite anodes, Green.energy.environ. 9 (6) (2024) 1027–1034, https://doi.org/10.1016/j.gee.2022.11.003.

[48] C. Yi, Y. Yang, T. Zhang, X. Wu, W. Sun, L. Yi, A green and facile approach for regeneration of graphite from spent lithium ion battery, J.clean.prod. 277 (2020) 123585, https://doi.org/10.1016/j.jclepro.2020.123585.
[49] Y. Zhang, L. Wang, H. Xu, J. Cao, D. Chen, W. Han, 3D Chemical Cross-Linking Structure of Black Phosphorus@CNTs Hybrid as a Promising Anode Material for Lithium Ion Batteries, Adv.funct.mater. 30 (12) (2020) 1909372, https://doi.org/10.1002/adfm.201909372.
[50] T. Zhang, T. Zhang, F. Wang, F. Ran, High-efficiently doping nitrogen in kapok fiber-derived hard carbon used as anode materials for boosting rate performance of sodium-ion batteries, J.energy.chem. 96 (2024) 472–482, https://doi.org/10.1016/j.jechem.2024.05.005.
[51] D. Feng, Y. Jiao, P. Wu, Proton-Reservoir Hydrogel Electrolyte for Long-Term Cycling Zn/PANI Batteries in Wide Temperature Range, Angew.chem.int.edit. 62 (1) (2023) e202215060, https://doi.org/10.1002/anie.202215060.
[52] L. Wang, J.-J. Lu, S.-Y. Li, F.-S. Xi, Z.-Q. Tong, X.-H. Chen, K.-X. Wei, W.-H. Ma, Controllable Interface Engineering for the Preparation of High Rate Silicon Anode, Adv.funct.mater. (2024) 2403574, https://doi.org/10.1002/adfm.202403574.